Application of Microwave Imaging for Brain Diagnostics

Marija Nikolic Stevanovic, Darko Ninkovic, Tushar Singh, Branislav Ninkovic, Miodrag Tasic, and Branko Kolundzija

***Abstract*— We present the application of the distorted Born iterative method for permittivity estimation of a realistic human phantom, which is an essential step in microwave medical diagnostics. Permittivity reconstruction is a difficult task due to the complexity of the electromagnetic model and the ill-posedness of the inverse scattering problems. Assuming that prior knowledge of the head anatomy is available from other imaging modalities, such as magnetic resonance imaging, we showed that electromagnetic tissue parameters could be accurately estimated even for tissues deeply located in the head. In our implementation of DBIM, we have gradually improved the estimation accuracy by initializing more complex models with results obtained for simpler models.**

***Index Terms*—Microwave imaging, inverse scattering, distorted Born iterative method, human phantoms.**

I. Introduction

In the last decade, the application of microwaves in medical diagnostics has gained much attention. The advantages of medical microwave imaging (MMWI) are non-invasiveness, low cost, utilization of nonionizing radiation, and ease of portability. However, due to the relatively low resolution of MMWI, it is envisioned primarily as a complementary screening tool for medical applications [1]–[3].

The gold standards in medical diagnostics are magnetic resonance imaging (MRI), computed tomography (CT), and positron emission tomography (PET) [4], [5], which produce high-resolution images with well-resolved tissues. However, their application is usually limited to large medical centers due to their high cost, and they are not appropriate for bedside monitoring. Additionally, CT and PET scans utilize harmful ionizing radiation.

The essential elements of any MMWI system are an antenna array, a reconstruction algorithm based on inverse scattering, and a reliable efficient 3D electromagnetic solver. Additionally, realistic human models (phantoms) are necessary for designing and testing MMWI systems.

Microwave imaging algorithms are generally classified into two categories: qualitative and quantitative. The goal of qualitative algorithms in medical imaging is to detect possible lesions or other tissues changes between measurements. They cannot infer the electromagnetic properties of the changes; instead, they estimate their location and shape. Examples of qualitative imaging algorithms are truncated singular value decomposition (TSVD) [6] and the linear sampling method (LSM) [7]. In contrast, quantitative algorithms reconstruct the complex permittivity in the whole domain of interest. Since different tissues have different electromagnetic properties, permittivity maps are also images of particular body parts.

Solving quantitative algorithms is difficult due to the complex scattering phenomenon. They are non-linear and ill-posed, making them prone to false solutions and more computationally intensive than qualitative algorithms. Examples are the inexact Newton methods [8] and the distorted Born iterative method (DBIM) [9], [10].

In this paper, we study the application of the DBIM to the permittivity reconstruction of a realistic head phantom. Although the utilized method is well-established, there are only a few examples of its application to realistic 3D human models. The main reasons for this are the non-uniqueness of the solution, the lack of detailed anatomical models adapted for electromagnetic analysis, and the extremely long computational time. The goal of this work is to test the algorithm's ability to estimate tissues' permittivities. Thus, we assume that the tissue boundaries are available, e.g., from a prior MRI screening. To initialize the algorithm, we first compute the average permittivity of the head.

The paper is organized as follows. After the introduction, we explain the DBIM in Section II. Section III describes the numerical examples and presents the obtained results. Finally, in the concluding section, we summarize the obtained results and give guidelines for future work.

II. Distorted Born Iterative Method

The goal of quantitative microwave imaging is to estimate the complex permittivity of the unknown object or the whole domain of interest. Fig. 1 illustrates a three-dimensional (3D) microwave imaging scenario consisting of an unknown non-magnetic inhomogeneous object, which occupies a volume v' and has the permittivity ε. The object is located in a known non-magnetic background medium whose permittivity is ε_b.

M. Nikolic Stevanovic is with the School of Electrical Engineering, University of Belgrade, Serbia (e-mail: mnikolic@etf.bg.ac.rs).

D. Ninkovic is with the School of Electrical Engineering, University of Belgrade, Serbia (e-mail: darko@etf.bg.ac.rs).

T. Singh is with WIPL-D d.o.o. Belgrade, Serbia and the School of Electrical Engineering, University of Belgrade, Serbia (e-mail: tushar.singh@wipl-d.com).

B. Ninkovic is with WIPL-D d.o.o. Belgrade, Serbia (e-mail: branislav.ninkovic@wipl-d.com).

M. Tasic is with the School of Electrical Engineering, University of Belgrade, Serbia (e-mail: tasic@etf.bg.ac.rs).

B. Kolundzija is with WIPL-D d.o.o. Belgrade, Serbia and School of Electrical Engineering, University of Belgrade, Serbia (e-mail: branko.kolundzija@wipl-d.com)

 ISBN 978-86-7466-930-3

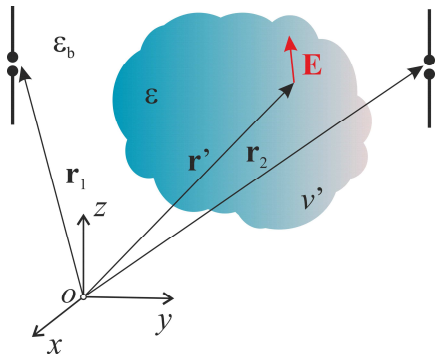

Fig. 1. Measurement scenario.

The measurements are taken by an array consisting of M antennas, out of which only two are shown in Fig. 1. The differential transmission coefficient between the i-th and the j-th antenna due to the presence of the object is given by [11]:

$$\Delta s_{ji} = -\frac{\mathrm{j}\omega}{2a_i a_j}\int_{v'} \Delta\varepsilon(\mathbf{r}')\,\mathbf{E}^j(\mathbf{r}';\varepsilon_\mathrm{b})\cdot\mathbf{E}^i(\mathbf{r}';\varepsilon)\mathrm{d}v', \tag{1a}$$

$$\Delta s_{ji} = s_{ji}(\varepsilon) - s_{ji}(\varepsilon_\mathrm{b}),\ i,j=1,\ldots,M, \tag{1b}$$

$$\Delta\varepsilon(\mathbf{r}') = \varepsilon(\mathbf{r}') - \varepsilon_\mathrm{b}(\mathbf{r}') \tag{1c}$$

where ω is the angular frequency, $s_{ji}(\varepsilon)$ is the transmission coefficients computed (or measured) in the presence of the scatterer, $s_{ji}(\varepsilon_\mathrm{b})$ is the transmission coefficient computed when the object is removed and substituted by the background medium, $\mathbf{r}'$ is the position vector of a point inside the object, $\mathbf{E}^j(\mathbf{r}';\varepsilon_\mathrm{b})$ is the electric field vector produced by the j-th antenna at $\mathbf{r}'$ in the background medium (the incident field), $\mathbf{E}^i(\mathbf{r}';\varepsilon)$ is the electric field vector produced by the i-th antenna at $\mathbf{r}'$ when the object is present (the total field), a_i and a_j are the complex amplitudes of the incident power waves at the i-th and j-th port, respectively.

If the estimate of the target permittivity ($\hat{\varepsilon}$) is utilized instead of the background permittivity (ε_b), (1) becomes

$$\Delta s_{ji} = -\frac{\mathrm{j}\omega}{2a_i a_j}\int_{v'} \Delta\varepsilon(\mathbf{r}')\,\mathbf{E}^j(\mathbf{r}';\hat{\varepsilon})\cdot\mathbf{E}^i(\mathbf{r}';\varepsilon)\mathrm{d}v', \tag{2a}$$

$$\Delta s_{ji} = s_{ji}(\varepsilon) - s_{ji}(\hat{\varepsilon}),\ i,j=1,\ldots,M, \tag{2b}$$

$$\Delta\varepsilon(\mathbf{r}') = \varepsilon(\mathbf{r}') - \hat{\varepsilon}(\mathbf{r}'). \tag{2c}$$

Since the object permittivity is unknown, the Born approximation is utilized, $\mathbf{E}^i(\mathbf{r}';\varepsilon)\approx\mathbf{E}^i(\mathbf{r}';\hat{\varepsilon})$. Thus, (2a) becomes

$$\Delta s_{ji} \approx -\frac{\mathrm{j}\omega}{2a_i a_j}\int_{v'} \Delta\varepsilon(\mathbf{r}')\,\mathbf{E}^j(\mathbf{r}';\hat{\varepsilon})\cdot\mathbf{E}^i(\mathbf{r}';\hat{\varepsilon})\mathrm{d}v'. \tag{3}$$

In the limit when $\hat{\varepsilon}\approx\varepsilon$, the left-hand side of (3) approaches zero. The equation (3) is fundamental for DBIM.

In order to apply DBIM, it is necessary to divide the domain of interest into smaller domains (voxels), v_k, $k=1,\ldots,L$. We assume that all voxels have the same volume ΔV, which has to be sufficiently small so that the permittivity is approximately constant in each voxel. We use ε_k and $\hat{\varepsilon}_k$ to denote the true and estimated complex permittivity of the k-th voxel.

DBIM is an iterative algorithm that needs to be initialized. If there is no prior knowledge about the permittivity of the inspected object, typically, the background permittivity is utilized, i.e., $\varepsilon_k^{(1)} = \varepsilon_{\mathrm{b},k}$, where $\varepsilon_{\mathrm{b},k}$ is the permittivity of the background medium in the k-th voxel and the superscript (1) denotes the iteration number. In the i-th iteration, the linear system of equations is

$$\Delta\mathbf{s}^{(i)} = \mathbf{L}^{(i)}\Delta\boldsymbol{\varepsilon}^{(i)}, \tag{4}$$

where $\Delta\mathbf{s}^{(i)}$ is a known vector whose elements are differences of the scattering parameters,

$$\Delta\mathbf{s}^{(i)} = \left[\Delta s_{1,1}^{(i)} \quad \Delta s_{1,2}^{(i)} \quad \cdots \quad \Delta s_{M,M}^{(i)}\right]^\mathrm{T}, \tag{5a}$$

$$\Delta s_{ij}^{(i)} = s_{ij}(\boldsymbol{\varepsilon}) - s_{ij}(\hat{\boldsymbol{\varepsilon}}^{(i)}),\ i,j=1,\ldots,M, \tag{5b}$$

$\hat{\boldsymbol{\varepsilon}}^{(i)}$ is the current permittivity estimate

$$\hat{\boldsymbol{\varepsilon}}^{(i)} = \left[\hat{\varepsilon}_1^{(i)} \quad \hat{\varepsilon}_2^{(i)} \quad \cdots \quad \hat{\varepsilon}_L^{(i)}\right]^\mathrm{T}, \tag{6}$$

$\mathbf{L}^{(i)}$ is the system matrix

$$\mathbf{L}^{(i)} = -\frac{\mathrm{j}\omega\Delta V}{2}\cdot \begin{bmatrix} \dfrac{\mathbf{E}^1(\mathbf{q}_1;\hat{\boldsymbol{\varepsilon}}^{(i)})\cdot\mathbf{E}^1(\mathbf{q}_1;\hat{\boldsymbol{\varepsilon}}^{(i)})}{a_1 a_1} & \cdots & \dfrac{\mathbf{E}^1(\mathbf{q}_L;\hat{\boldsymbol{\varepsilon}}^{(i)})\cdot\mathbf{E}^1(\mathbf{q}_L;\hat{\boldsymbol{\varepsilon}}^{(i)})}{a_1 a_1} \\ \dfrac{\mathbf{E}^1(\mathbf{q}_1;\hat{\boldsymbol{\varepsilon}}^{(i)})\cdot\mathbf{E}^2(\mathbf{q}_1;\hat{\boldsymbol{\varepsilon}}^{(i)})}{a_1 a_2} & \cdots & \dfrac{\mathbf{E}^1(\mathbf{q}_L;\hat{\boldsymbol{\varepsilon}}^{(i)})\cdot\mathbf{E}^2(\mathbf{q}_L;\hat{\boldsymbol{\varepsilon}}^{(i)})}{a_1 a_2} \\ \vdots & \cdots & \vdots \\ \dfrac{\mathbf{E}^M(\mathbf{q}_1;\hat{\boldsymbol{\varepsilon}}^{(i)})\cdot\mathbf{E}^M(\mathbf{q}_1;\hat{\boldsymbol{\varepsilon}}^{(i)})}{a_M a_M} & \cdots & \dfrac{\mathbf{E}^M(\mathbf{q}_l;\hat{\boldsymbol{\varepsilon}}^{(i)})\cdot\mathbf{E}^M(\mathbf{q}_L;\hat{\boldsymbol{\varepsilon}}^{(i)})}{a_M a_M} \end{bmatrix}, \tag{7}$$

and $\Delta\boldsymbol{\varepsilon}^{(i)}$ is an unknown vector

$$\Delta\boldsymbol{\varepsilon}^{(i)} = \left[\Delta\varepsilon_1^{(i)} \quad \Delta\varepsilon_2^{(i)} \quad \cdots \quad \Delta\varepsilon_L^{(i)}\right]^\mathrm{T}, \tag{8}$$

whose elements are the permittivity updates. The system (4) is solved by means of truncated singular value decomposition. The regularized solution is

$$\Delta\boldsymbol{\varepsilon}^{(i)} = \sum_{n=1}^{n_\mathrm{max}} \frac{1}{\sigma_i}\left(\mathbf{u}_n^\mathrm{H}\cdot\Delta\mathbf{s}^{(i)}\right)\mathbf{v}_n, \tag{9}$$

where $\mathbf{u}_n$, $\mathbf{v}_n$ are the singular vectors of matrix $\mathbf{L}^{(i)}$, σ_i are the corresponding singular values, and n_max is the truncation index, obtained from the condition $10\log_{10}(\sigma_{n_\mathrm{max}}/\sigma_1) < -20$ dB. The permittivity estimate in the next iteration is obtained as

 ISBN 978-86-7466-930-3

$$\hat{\boldsymbol{\varepsilon}}^{(i+1)} = \hat{\boldsymbol{\varepsilon}}^{(i)} + \Delta\hat{\boldsymbol{\varepsilon}}^{(i)}, \tag{9}$$

The iterative algorithm terminates when the magnitude of each member of the vector $\Delta\boldsymbol{\varepsilon}^{(i)}$ is smaller than some predefined value.

In some cases, prior knowledge about the tissue is available, i.e., from MRI scans. In these situations, we estimate the tissue permittivity, assuming that their surface boundaries are known. Thus, we can reduce the number of unknowns to the number of tissues. The measurement model becomes

$$\Delta\mathbf{s}^{(i)} = \mathbf{L}^{(i)}\mathbf{H}\,\Delta\boldsymbol{\varepsilon}^{(i)}, \tag{10}$$

where $\mathbf{H}$ is the transformational matrix of size $L\times N$, and N is the number of tissues. The (k,j) element of $\mathbf{H}$ is one if v_k belongs to j-th domain and zero otherwise. The unknown vector is now

$$\Delta\boldsymbol{\varepsilon}^{(i)} = \left[\Delta\varepsilon_1^{(i)} \quad \Delta\varepsilon_2^{(i)} \quad \cdots \quad \Delta\varepsilon_N^{(i)}\right]^{\mathrm{T}}, \tag{11}$$

where $\Delta\varepsilon_j^{(i)}$ refers to the j-th domain.

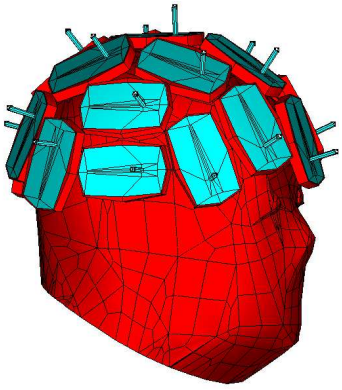

Fig. 2. Head model and the antenna array.

III. Numerical Results

In order to test the DBIM algorithm, we considered a realistic head model derived from the NEVA woman model [12]–[14]. The antenna array consisted of 21 identical microstrip trapezoidal patch antennas described in [12]. The antennas were fed by coaxial cables as illustrated in Fig. 2. The operating frequency of the array was 1 GHz, as this frequency is found to be the optimal in terms of both penetration depth and resolution.

The forward simulations were computed using the full-wave electromagnetic solver WIPL-D Pro [15]. All results presented in this paper are generated using a desktop computer: Intel Core i7-9700 CPU @3 GHz, NVIDIA GeForce GTX 750 Ti GPU, with 32 GB of RAM under the Windows 10 operating system.

In the first example, the goal was to find the equivalent homogeneous head phantom, which is equivalent (in terms of scattering parameters) to the realistic head phantom comprising seven tissues (skin, fat, mucous membrane, skull, gray matter, white matter and cerebellum).

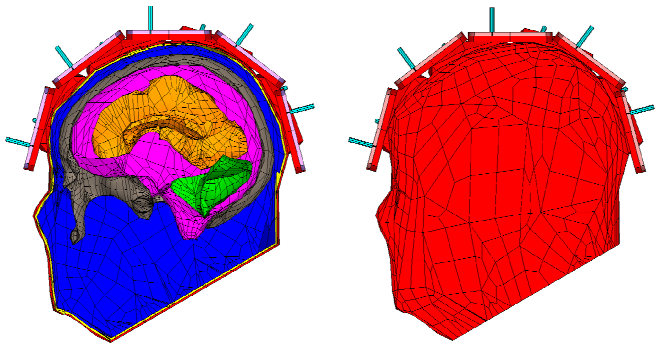

(a) (b)

Fig. 3. (a) Reference head model with seven tissues. (b) Equivalent homogeneous head model filled with the average tissue.

The head interior was divided into $L = 8676$ voxels. As there was only one domain (averaged tissue), the transformation matrix $\mathbf{H}$ was a column vector of size $L\times 1$ with all elements being equal to one. As the initial permittivity estimate, we used the value calculated by the standard averaging procedure $\varepsilon_r^{(1)} = 41.47 - \mathrm{j}14.15$ [12]. After six iterations, the permittivity value converged to $\varepsilon_r^{(6)} = 34.64 - \mathrm{j}12.68$. As a comparison, the gradient optimization [12] yielded for the average tissue permittivity $\varepsilon_r = 34.68 - \mathrm{j}12.68$, which is almost the same result. The number of unknowns in the WIPL-D model (current coefficients) for this example was 24109, and an iteration lasted about 6 minutes.

In the second scenario, the goal was to reconstruct the permittivities of five tissues (skin, fat, mucous membrane, skull, and gray matter) from the head model shown in Fig. 4, assuming that the tissue boundaries are known. As the initial permittivity, we used the value obtained in the first experiment, $\varepsilon_r^{(1)} = 34.64 - \mathrm{j}12.68$, for all tissues.

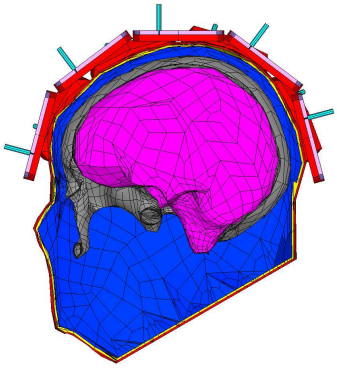

Fig. 4. Model with five tissues.

The WIPL-D model with five tissues has 48354 unknowns and each iteration lasted about 55 minutes. The results obtained after 20 iterations of the algorithm are shown in Table I. The true permittivities of tissues are given in the second column, and the estimated permittivities are shown in the third column. The last column indicates the number of voxels per each tissue.

 ISBN 978-86-7466-930-3

TABLE I. ESTIMATION RESULTS FOR THE HEAD WITH FIVE TISSUES

Tissue Name	ε_r	$\varepsilon_r^{(20)}$	**Number of voxels**
Skin	45.71 – j15.84	45.79 – j15.82	3445
Fat	11.29 – j2.09	11.27 – j2.17	5086
Mucous Membrane	45.66 – j15.95	45.64 – j15.94	35340
Grey Matter	52.28 – j17.71	52.28 – j17.71	18267
Skull Bone	20.58 – j6.54	20.59 – j6.55	7179

In the last example, the goal was to reconstruct the permittivities of the head phantom with seven tissues (Fig. 3a), assuming that the tissue boundaries are known. Again, all elements of the vector $\boldsymbol{\varepsilon}^{(1)}$ were initialized with the averaged tissue value $\varepsilon_r = 34.64 - j12.68$. Firstly, we ran the algorithm with a smaller number of voxels for 20 iterations, and each of them lasted about 60 minutes. We used the obtained results as the initial guess for the permittivities for the next 10 iterations with an increased number of voxels. The execution time of each of those iterations was about 105 minutes. The number of unknowns in the WIPL-D model for this scenario was 60778. Table II shows the results obtained after all 30 iterations.

TABLE II. ESTIMATION RESULTS FOR THE HEAD WITH SEVEN TISSUES

Tissue Name	ε_r	$\varepsilon_r^{(30)}$	**Number of voxels**
Skin	45.71 – j15.84	45.69 – j15.85	463/3445
Fat	11.29 – j2.09	11.33 – j2.03	655/5086
Mucous Membrane	45.66 – j15.95	45.73 – j15.92	4480/35340
Grey Matter	52.28 – j17.71	52.42 – j17.91	1690/13285
Skull Bone	20.58 – j6.54	20.67 – j6.70	903/7179
White Matter	38.58 – j11.18	38.33 – j11.27	492/3864
Cerebellum	48.86 – j23.51	34.66 – j12.65	140/1118

The biggest error was obtained for the cerebellum permittivity, which is the smallest domain located deep inside the head. The estimated permittivity values are shown in Fig. 5 (dots at the end represent the true values). Moreover, it can be observed that the cerebellum permittivity has changed insignificantly. Thus, we ran additional 10 iterations of DBIM for estimating the permittivity of the cerebellum, while the permittivities of other six tissues were fixed to the values obtained after 30 iterations. Finally, the permittivity of the cerebellum converged closely to the true value ($\varepsilon_r^{(40)} = 48.80 - j23.51$).

IV. CONCLUSION

We studied the capability of the DBIM to estimate the permittivities of tissues in realistic human head phantoms. We considered phantoms of different complexity and utilized the simplest model to initialize more elaborate ones. The permittivity was accurately estimated under the assumption that tissue boundaries are known. We will consider the case in which no prior knowledge is available in future work. However, voxel-based meshing has to be utilized in that case, which yields a significantly larger number of unknowns in the forward electromagnetic model and, consequently, increases the computational time enormously.

ACKNOWLEDGMENT

This work was supported by the EMERALD project funded from the European Union's Horizon 2020 research and innovation program under the Marie Skłodowska-Curie grant agreement No. 764479.

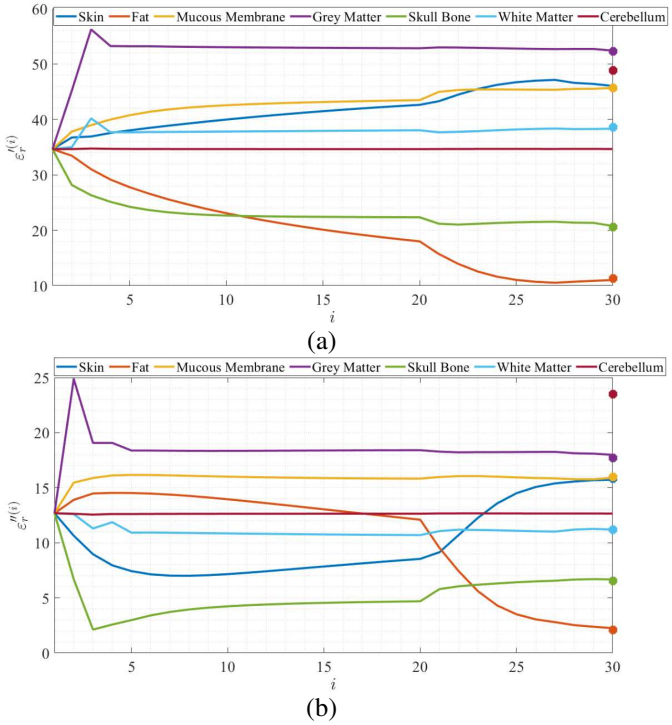

Fig. 5. Estimated permittivites of tissues for each iteration. (a) Real and (b) imaginary part of the complex permittivity.

REFERENCES

[1] R. Chandra, H. Zhou, I. Balasingham and R. M. Narayanan, "On the Opportunities and Challenges in Microwave Medical Sensing and Imaging," *IEEE Transactions on Biomedical Engineering*, vol. 62, no. 7, pp. 1667-1682, July 2015.

[2] L. Crocco, I. Karanasiou, M. James, R. Conceição, "Emerging Electromagnetic Technologies for Brain Diseases Diagnostics, Monitoring and Therapy," *Springer*, Cham, Switzerland, 2018.

[3] R. Conceição, J. Mohr, M. O'Halloran, "An Introduction to Microwave Imaging for Breast Cancer Detection," Switzerland, Springer, 2018.

[4] G. Zhu, A. Bialkowski, L. Guo, B. Mohammed and A. Abbosh, "Stroke Classification in Simulated Electromagnetic Imaging Using Graph Approaches," *IEEE Journal of Electromagnetics, RF and Microwaves in Medicine and Biology*, vol. 5, no. 1, pp. 46-53, March 2021.

[5] A. S. M. Alqadami, A. Trakic, A. E. Stancombe, B. Mohammed, K. Bialkowski and A. Abbosh, "Flexible Electromagnetic Cap for Head

 ISBN 978-86-7466-930-3

Imaging," *IEEE Transactions on Biomedical Circuits and Systems*, vol. 14, no. 5, pp. 1097-1107, Oct. 2020.

[6] J. D. Shea, B. D. Van Veen and S. C. Hagness, "A TSVD Analysis of Microwave Inverse Scattering for Breast Imaging," *IEEE Transactions on Biomedical Engineering*, vol. 59, no. 4, pp. 936-945, April 2012.

[7] L. Crocco, I. Catapano, L. Di Donato and T. Isernia, "The Linear Sampling Method as a Way to Quantitative Inverse Scattering," *IEEE Transactions on Antennas and Propagation*, vol. 60, no. 4, pp. 1844-1853, April 2012.

[8] G. Bozza, C. Estatico, M. Pastorino, and A. Randazzo, "An Inexact Newton Method for Microwave Reconstruction of Strong Scatterers," in *IEEE Antennas and Wireless Propagation Letters*, vol. 5, pp. 61-64, 2006.

[9] L. Guo, N. Nguyen-Trong, A. AI-Saffar, A. Stancombe, K. Bialkowski and A. Abbosh, "Calibrated Frequency-Division Distorted Born Iterative Tomography for Real-Life Head Imaging," in IEEE Transactions on Medical Imaging, doi: 10.1109/TMI.2021.3132000.

[10] L. Guo, M. Khosravi-Farsani, A. Stancombe, K. Bialkowski and A. Abbosh, "Adaptive Clustering Distorted Born Iterative Method for Microwave Brain Tomography With Stroke Detection and Classification," in IEEE Transactions on Biomedical Engineering, vol. 69, no. 4, pp. 1512-1523, April 2022.

[11] Nikolova, N. Introduction to Microwave Imaging, EuMA High Frequency Technologies Series, Cambridge University Press, Cambridge.

[12] T. Singh et al., "New Method for Calculation of Average Electric Properties of Reference Head Phantom in Microwave Imaging," 2022 16th European Conference on Antennas and Propagation (EuCAP), 2022, pp. 1-5.

[13] S. N. Makarov, G. M. Noetscher, J. Yanamadala, M. W. Piazza, AU - S. Louie, A. Prokop, A. Nazarian, A. Nummenmaa "Virtual Human Models for Electromagnetic Studies and Their Applications," in *IEEE Reviews in Biomedical Engineering*, vol. 10, pp. 95-121, 2017, doi: 10.1109/RBME.2017.2722420.

[14] https://www.nevaelectromagnetics.com/

[15] WIPL-D Pro v17 [Online]. Available: http://www.wipl-d.com/.

 ISBN 978-86-7466-930-3